Simulation of Scanning Tunneling Microscope Images of 1,3-Cyclohexadiene Bound to a Silicon Surface

M. Galperin[†] and D. N. Beratan*

Departments of Chemistry and Biochemistry, Duke University, Durham, North Carolina 27708

Received: September 16, 2004; In Final Form: November 10, 2004

Scanning tunneling microscope (STM) images of 1,3-cyclohexadiene bound to silicon are interpreted using a nonequilibrium Green's function method. The resolution of the carbon−carbon double bond for positive bias voltages but not for negative bias voltages is explained using a quasiprobability density analysis. The asymmetry in the images arises from the system's voltage dependent electronic structure. A π^* orbital is found to be responsible for the empty state STM images of the carbon−carbon double bond, which is observed experimentally. The π orbital relevant for the opposite bias does not produce an STM image sharply localized in the bond region because the molecule induces a Si-surface dipole dependent on the bias. The dipole voltage dependence arises from molecular charging. This result emphasizes the importance of simulating the molecule as an element in an open quantum system.

1. Introduction

Molecular electronics has gained considerable attention with the emergence of proximal probe techniques and theoretical methods that allow the structure and transport properties of molecules and molecular assemblies to be interrogated.[1−7] Progress toward developing molecule-based devices may arise from an ability to control molecular junctions, heating, conformational stability, and switching.[8−12] Theory is providing tools capable of describing these open nonequilibrium quantum systems. Beginning with current calculation within tight-binding models by Caroli and co-workers[13−15] using nonequilibrium Green's function (NEGF) methods,[16,17] the NEGF approach has become one of the key techniques to describe open nonequilibrium quantum systems. Initial applications of this method to compute the conductivity of single molecules were reported by the groups of Datta[18,19] and Guo.[20−22]

Among the most important challenges in molecular devices is the desire to describe a molecule's response to an applied bias. Electron−electron interactions on the molecular bridge (between the contacts), molecular charging, and the potential profile across the junction all influence the device characteristics. Each of these issues can be explored within the NEGF Hartree−Fock (HF) approach.[23,24]

Here, we apply the NEGF-HF method to interpret STM experiments on 1,3-cyclohexadiene bound to silicon (100) 2 × 1 surfaces.[25,26] In the experiment, STM imaging was used to investigate the reaction of 1,3-cyclohexadiene with Si dimers on the bare Si(100) surface. Among the conformers reported, we choose the [4+2] intradimer A (see ref 25) for our simulations. An empty state image—a situation when transport is governed by the LUMO and higher energy orbitals—shows two well-defined maxima (see Figure 2A in ref 25), ascribed by the authors to the carbon−carbon double bond. Experiments were done at 300 K. Clear STM images of the bond were observed only for electron flow from tip to substrate (−1.3 V tip bias). Here, presumably, the current-carrying orbitals include the LUMO and higher energy unoccupied orbitals. For the opposite voltage bias, no clear image of the bond was obtained.[25−27] In this paper we explore the physical origins of the STM images and their strong dependence on bias voltage, as a simple closed system molecular orbital view of the adsorbate is not sufficient to explain the STM images.

Early studies of adsorbed molecules in STM geometry[28,29] utilized a scattering theory formalism as a theoretical tool. As a result, the influence of the contact population (Pauli principle) is disregarded in these works. Furthermore, the NEGF based formalism, though not implemented in the manuscript, can be readily generalized beyond the HF (mean field) level of theory, whereas scattering theory consideration is mean field (effective potential) by its nature.

2. Method

The experimental system consists of a tungsten tip, silicon (100) 2×1 substrate, and bound organic molecule (1,3-cyclohexadiene). We separate the system into left and right electrodes (or contacts, which are treated as reservoirs of free carriers, each in equilibrium) and a molecule (or supermolecule). The nonequilibrium physics is assumed to occur only in the molecule (or supermolecule) region. Interactions included in the model are couplings between the molecule and the contacts, electron−electron interactions in the molecule, and the influence of the external electrostatic potential (computed using Laplace's equation) on the molecule. For a planar geometry of electrodes, the electrostatic potential is a linear ramp. The Hamiltonian for the full system is

$$\hat{H} = \hat{H}_0 + \hat{V}$$

$$\hat{H}_0 = \sum_{i,j;\sigma} H^{c}_{ij}\hat{c}^{\dagger}_{i;\sigma}\hat{c}_{j;\sigma} + \sum_{k\in L,R;\sigma} \epsilon_k \hat{c}^{\dagger}_{k;\sigma}\hat{c}_{k;\sigma}$$

$$\hat{V} = \sum_{i,j;\sigma} V^{\mathrm{ext}}_{ij}\hat{c}^{\dagger}_{i;\sigma}\hat{c}_{j;\sigma} + \frac{1}{2}\sum_{\substack{i_1,i_2,i_3,i_4\\ \sigma,\sigma'}} V^{i_1 i_2}_{i_3 i_4}\hat{c}^{\dagger}_{i_1;\sigma}\hat{c}^{\dagger}_{i_2;\sigma'}\hat{c}_{i_4;\sigma'}\hat{c}_{i_3;\sigma} + \sum_{k\in L,R;i;\sigma} (V_{ki}\hat{c}^{\dagger}_{k;\sigma}\hat{c}_{i;\sigma} + \mathrm{hc}) \quad (1)$$

[†] Current address: Department of Chemistry, Northwestern University, Evanston, IL 60208.

10.1021/jp045783f CCC: $30.25
Published on Web 01/11/2005

where the *i* and *j* indices are used for the Löwdin (orthogonalized atomic) orbitals of the molecule,[30] and *k* denotes electronic states of the left (*L*) and right (*R*) contacts. The spin index is σ. Below, we treat $\hat{H}_0$ as a zero-order Hamiltonian and $\hat{V}$ as a perturbation. The core Hamiltonian matrix elements H^{c}_{ij} and two-center integrals $V^{i_1 i_2}_{i_3 i_4}$ are taken from Gaussian[31] calculations on the supermolecule, although one could compute the integrals by other means.[32]

The influence of the external (contacts) relative to the supermolecule part of the system as well as the result of the interaction on the molecule (external potential and electron−electron interaction) is expressed in terms of a self-energy. We assume that the total self-energy (computed by projecting the problem onto the molecular subspace) is the sum of the self-energies arising from coupling to the contacts, interaction with the external potential, and electron−electron interactions in the molecule. Though self-energies due to coupling to the contacts and interaction with the external potential can be obtained exactly for this Hamiltonian, the electron−electron interactions must be treated approximately. We include electron−electron interactions to first order in the expansion of the evolution operator

$$\hat{S} = \hat{T}_{\mathrm{c}} \exp\left[-\frac{\mathrm{i}}{\hbar}\int_c \mathrm{d}\tau\ \hat{V}_{\mathrm{I}}(\tau)\right] \tag{2}$$

where *c* is the integration contour, $\hat{T}_{\mathrm{c}}$ is the contour ordering operator and $\hat{V}_{\mathrm{I}}(\tau)$ is the perturbation in the interaction picture on the contour relative to the zero-order Hamiltonian $\hat{H}_0$ (1)

$$\hat{V}_{\mathrm{I}}(\tau) = \exp\left[\frac{\mathrm{i}}{\hbar}\hat{H}_0\tau\right]\hat{V}\exp\left[-\frac{\mathrm{i}}{\hbar}\hat{H}_0\tau\right] \tag{3}$$

This leads to the Hartree−Fock level description of electron−electron interactions in the molecule. Because we are interested in steady-state currents, a Keldysh contour analysis is sufficient, and projection to the real-time axis requires that we solve the coupled Dyson and Keldysh equations self-consistently.[33,34] After Fourier transforming to the energy domain, these equations are

$$\mathbf{G}^{\mathrm{r}}(E) = [E - \mathbf{H}_0 - \Sigma^{\mathrm{r}}]^{-1} \tag{4}$$

$$\mathbf{G}^{<}(E) = \mathbf{G}^{\mathrm{r}}(E)\,\Sigma^{<}(E)\,\mathbf{G}^{a}(E) \tag{5}$$

Here, $\mathbf{G}^{\mathrm{r}}(E)$ is the retarded Green function (GF), $\mathbf{G}^{\mathrm{a}}(E) = [\mathbf{G}^{\mathrm{r}}(E)]^{\dagger}$ is the advanced GF, $\mathbf{G}^{<}$ is the lesser GF, and $\mathbf{H}_0$ is the molecular part of the operator $\hat{H}_0$ in eq 1. Σ^{r} and $\Sigma^{<}(E)$ are the retarded and lesser projections of the self-energy (SE), respectively. These are assumed to be sums of contributions due to coupling to the contacts and, for the retarded SE, interaction with the external potential

$$[\Sigma_{\mathrm{ext}}]_{ij} = V^{\mathrm{ext}}_{ij} \tag{6}$$

and electron−electron interaction (Hartree−Fock self-energy)

$$[\Sigma_{\mathrm{HF}}]_{ij;\sigma} = \sum_{k,m}(V^{ik}_{jm}[\rho_{mk,\sigma} + \rho_{mk,\bar{\sigma}}] - V^{ik}_{mj}\rho_{mk,\sigma}) \tag{7}$$

where $\bar{\sigma}$ is the opposite spin projection of σ.

Because the density matrix used in the HF self-energy calculation in (7) is given by integration of the lesser GF

$$\rho_{mk,\sigma} = -i\int_{-\infty}^{+\infty}\frac{\mathrm{d}E}{2\pi}G^{<}_{mk,\sigma}(E) \tag{8}$$

the procedure becomes self-consistent. Self-consistent solution requires convergence of the HF self-energy (each element of the HF self-energy matrix). A detailed description of this approach appears in ref 24.

After convergence of the procedure, the current at a given voltage is calculated using the Landauer formula[34,35]

$$I = -\frac{2|e|}{\hbar}\int_{-\infty}^{+\infty}\frac{\mathrm{d}E}{2\pi}\mathrm{Tr}[\Gamma_{\mathrm{L}}(E)\,G^{\mathrm{r}}(E)\,\Gamma_{\mathrm{R}}(E)\,G^{\mathrm{a}}(E)] \times [f_{\mathrm{L}}(E) - f_{\mathrm{R}}(E)] \tag{9}$$

where the trace is over the molecular subspace and

$$\Gamma_{\mathrm{K}}(E) = \mathrm{i}[\Sigma^{\mathrm{r}}_{\mathrm{K}}(E) - \Sigma^{\mathrm{a}}_{\mathrm{K}}(E)] \qquad \mathrm{K} = \mathrm{L}, \mathrm{R} \tag{10}$$

This expression is appropriate for a HF-level description of the electron−electron interaction. In a more general case (e.g., when inelastic effects or electron correlations are included), a more general expression is needed.[33,36]

The main obstacle to treating large systems with the NEGF approach is the necessity to evaluate integrals over infinite (in practice, large) energy ranges at each step of the self-consistent procedure, as is seen from eq 8. This in turn leads to the necessity of using a fine energy grid and inverting large matrices to compute the retarded GF (see eq 4) at each point of the grid. The consideration can be simpler, however, in the wide-band limit, when the relevant molecular structure is coupled to a much wider continuum of electrode states; i.e., influence of the edges of bands (energy dependence of the corresponding self-energy) can be disregarded. In this case, and within a HF description of electron−electron interaction, one can replace the multiple matrix inversions by solving one eigenvalue problem and evaluating all the relevant integrals analytically (for example those in eqs 8 and 9), thus removing the need for an energy mesh. An eigenvalue problem is solved for a complex symmetric matrix consisting of the Hamiltonian of the supermolecule plus the retarded self-energy arising in our case from coupling to contacts, interaction with the external potential, and electron−electron interaction on the supermolecule. Details of this approach appear in ref 24.

Even with the approximations described above, full surface current maps are inaccessible. To explore the nature of the STM images, we instead analyze the probability density plot for the molecular orbital(s) that mediate the current flow—those orbitals that have an energy between the chemical potentials of the two electrodes. Following ref 37, we assume that the current flows mainly through the regions of space where the energetically accessible orbitals are localized. The reason for this assumption is the proportionality of the current to the spatial gradient of the wave function.[38] That is, the current is expected to be large in regions of rapidly varying probability density (i.e., in the localization region).

In closed quantum systems, the electron density is given by the absolute square of the wave function. The analogous density is nontrivial to define for an open quantum system. Indeed, the issue is complicated by the fact that the open-system Hamiltonian is complex (the Hamiltonian of the supermolecule plus the retarded self-energy). Thus, the eigenvalue problem involves a complex symmetric matrix **H**. As a consequence, the eigenvalues are complex. The real part represents molecular orbital (MO) energies and the imaginary part represents the broadening of the levels that arises from coupling to the contacts. One has to distinguish between left and right eigenvectors:

$$\hat{H}|\psi_i^{\mathrm{R}}\rangle = E_i|\psi_i^{\mathrm{R}}\rangle$$
$$\langle\psi_i^{\mathrm{L}}|\hat{H} = \langle\psi_i^{\mathrm{L}}|E_i \qquad (11)$$

here the $E_i = \epsilon_i - i\gamma_i$ (with $\gamma_i > 0$) values are complex and the functions $\langle\psi_i^{\mathrm{L}}|$ and $|\psi_i^{\mathrm{R}}\rangle$ are the corresponding left and right eigenvectors. The eigenvector inner product is

$$\langle\psi_i^{\mathrm{L}}|\psi_j^{\mathrm{R}}\rangle = \int \mathrm{d}\vec{r}\ \psi_i^{\mathrm{L}}{}^*(\vec{r})\ \psi_j^{\mathrm{R}}(\vec{r}) \qquad (12)$$

The orthonormality requirement

$$\langle\psi_i^{\mathrm{L}}|\psi_j^{\mathrm{R}}\rangle = \delta_{i,j} \qquad (13)$$

allows the definition of the complex quasiprobability density:

$$P_i(\vec{r}) = \psi_i^{\mathrm{L}}{}^*(\vec{r})\ \psi_i^{\mathrm{R}}(\vec{r}) \qquad (14)$$

introduced by Moiseyev.[39] Quasiprobability becomes the usual quantum mechanical probability density in the case of closed systems, when $P_i(\vec{r})$ is real. Following ref 39, we identify $\mathrm{Re}[P_i(\vec{r})]$ as a probability density for the case of an open system. Moreover, deviation of $\mathrm{Im}[P_i(\vec{r})]$ from zero is due to the presence of coupling between the molecule and the contacts (openness of the system). The effect of this coupling leads to the instability of the state (molecular orbital). A quantity that measures the local effective strength of MO coupling to the contacts is $\mathrm{Im}[P_i(\vec{r})]$. The larger $\mathrm{Im}[P_i(\vec{r})]$, the stronger is the coupling (facilitating current flow). We will use quasiprobability (its real and imaginary parts) as a tool to evaluate MO contributions to the STM image.

3. Application to 1,3-Cyclohexadiene on Silicon (100)

We applied the approach described above to simulate STM images of 1,3-cyclohexadiene attached to a Si(100) 2 × 1 surface probed with a tungsten tip. The tip is placed above the carbon−carbon double bond (see Figures 1 and 2). The supermolecule under study is a cluster of 10 silicon atoms bound to a 1,3-cyclohexadiene molecule in the motif of the experimentally modified reconstructed silicon surface with a single tungsten atom representing the tip. For details of relaxation of the molecular structure see refs 25 and 26. Effectiveness of the small Si cluster/MO approach in resolving details of molecular absorption is due to the extremely localized electronic and chemical nature of the Si surface.[40] Dangling bonds at the crystal side of the silicon cluster are capped by H atoms. The side of the cluster facing the molecule is not capped.[41] A planar geometry is assumed for contacts, which are treated in the wide-band limit (see Figure 1). Coupling to the contacts is taken to be mediated by all of the silicon atoms of the cluster as well as by capping H atoms (coupling to the left contact), and by the tungsten atom (coupling to the right contact). That is, the self-energy arising from coupling to the contacts is zero for all atoms except those indicated above. In our simulations we disregard the real part of the self-energy and take its imaginary part in the AO representation to be diagonal. For the orbitals of atoms taken to be coupled to the contacts we assume the wide-band limit for the self-energy. That is, we take the imaginary part to be a constant (energy independent) width chosen in our model as $\gamma = 0.2$ eV (an order of magnitude estimate of the inverse lifetime for the decay of an excess electron into continuum of states[42]).

The number of atoms included in the supermolecule is dictated by the memory requirements of the program. A one-atom tip approximation in the simulation of STM experiments is a common practice. The Tersoff−Hamann approach, for example, represents the tip by an s state on the outermost atom of the tip.[43,44] AOs are represented using the LANL2DZ[31] basis set. The Fermi energy is chosen to lie in the middle of the HOMO−LUMO gap of the unbiased supermolecule, $E_{\mathrm{F}} = -2.7211$ eV (-0.1 au). In general, the Fermi energy relative to the molecular eigenstates can be considered to be a parameter of the calculation for this model.

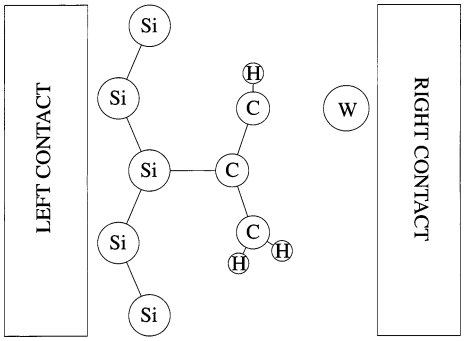

Figure 1. Edge view of the model used. The "supermolecule" is $W-C_6H_8-Si_{10}H_{12}$.

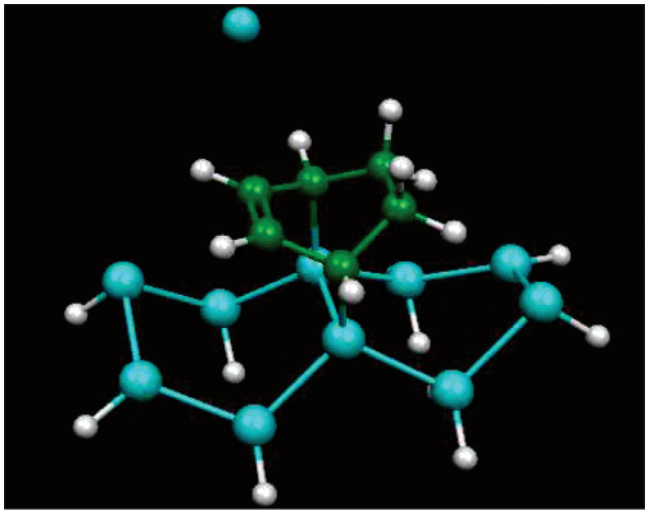

Figure 2. Model of the supermolecule.

An applied voltage V was assumed to change the position of the right (tungsten) chemical potential, whereas the left (silicon crystal) chemical potential remains unchanged ($\mu_{\mathrm{L}} = \mu_{\mathrm{Si}} = E_{\mathrm{F}}$) at all voltages. The reason for this is that the molecule is strongly coupled to the substrate whereas coupling to the tip is weak. As such, orbitals of the molecule are expected to shift in energy with the substrate potential. The chemical potential of the tip is assumed to move freely. Bias is measured as a difference between substrate (Si) and tip (W), i.e., $V = V_{\mathrm{Si}} - V_{\mathrm{W}}$. Because it is assumed that the chemical potential of the Si substrate does not change with the voltage relative to the molecular levels $\mu_{\mathrm{Si}} = E_{\mathrm{F}}$ or $V_{\mathrm{Si}} = 0$. The chemical potential of the W tip moves freely, i.e., $\mu_{\mathrm{W}} = E_{\mathrm{F}} - |e|V_{\mathrm{W}} = E_{\mathrm{F}} + |e|V$, where the electron charge is $e = -|e|$. As a result, at negative biases, $V < 0$, $\mu_{\mathrm{Si}} > \mu_{\mathrm{W}}$, and electron flow is from substrate to the tip with the HOMO and lower energy orbitals being the main current mediating orbitals. At positive biases ($V > 0$, $\mu_{\mathrm{Si}} < \mu_{\mathrm{W}}$), the flow is in the opposite direction and the main participating orbitals are the LUMO and higher energy orbitals. Calculations were performed for room-temperature systems.

This approach has numerous limitations. The most significant concern is the use of a wide-band limit for the contacts.

Although this approach is reasonable for metals, using it to describe the silicon contact is more questionable. A more rigorous approach would be to calculate the self-energies arising from the leads based on the surface Green functions. This computation could be implemented using, for example, a decimation technique.[45−47] Datta and co-workers[48] recently implemented calculations of this kind for a silicon contact. We suspect that, in our specific case, the details of the contact self-energy are of relatively minor importance, because the surface dipole relevant for the observed asymmetry is described correctly by the Si cluster included in the supermolecule (vide infra). Justification is provided by several closed system equilibrium runs done with the Gaussian package, where increasing the Si cluster size did not substantially change the charge distribution between the Si cluster and the molecule. Also, we are interested in the shape of the molecular orbitals (more precisely, the corresponding probability densities) that mediate current flow and the immediate molecule−crystal interface. These orbitals are localized on the molecule itself, and are nearly independent of the silicon substrate beyond interaction with the nearest silicon atoms (see results of the calculations presented below). The silicon cluster is taken as part of a supermolecule, generating part of the molecule−substrate interactions. Changing the number of silicon atoms in the cluster did not significantly change the observed results.

Another argument in favor of the wide-band approximation is the fact that the MOs of the isolated molecule are in the region below (for the HOMO and lower-energy orbitals) or above (for the LUMO and higher-energy orbitals) the silicon crystal band gap. Because the molecular structure is "fixed" relative to the band structure of silicon (a result of strong coupling because the molecule is attached to the silicon surface), the energetic situation favors the approximation. Essentially the same approximation (without opening the quantum system) is made in standard quantum chemical descriptions of STM (see, e.g., ref 49 and references therein). In those calculations, a finite cluster of silicon atoms (we include the cluster in the supermolecule) is assumed to represent the silicon contact, whereas the true band structure of crystalline silicon is usually ignored. In our analysis, we follow the same line of argument but add the effects arising from the open nature of the system and the nonequilibrium electronic population of the supermolecule.

The main advantage of using open rather than isolated cluster calculations is likely the freedom to allow charging of the molecule at different applied voltages. This leads to essential changes of the electronic structure. The electrostatic potential resulting from the spatial distribution of the charge plays an important role in facilitating or preventing electron tunneling through the junction at different voltage drops due to different barrier shapes, that the electron has to tunnel through. We treat charging effect in a self-consistent manner.

Finally, we stress that a qualitative picture consistent with the observed experimental results can be developed using this simplified approach.

4. Results

The current−voltage characteristics of the system are presented in Figure 3. One sees asymmetry in the current−voltage relation as a function of bias polarity (see discussion below). Note that large current enhancements are computed at voltages of ∼6 V, which is high compared to the experimental data. The reason for this discrepancy is that HF calculations overestimate the HOMO−LUMO gap 2−3-fold.[50] Neglect of image charge interactions with the contacts causes a further overestimate of

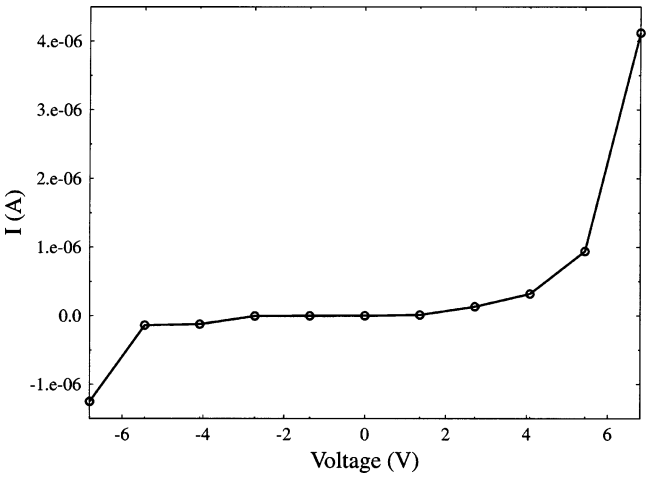

Figure 3. Calculated current−voltage relation.

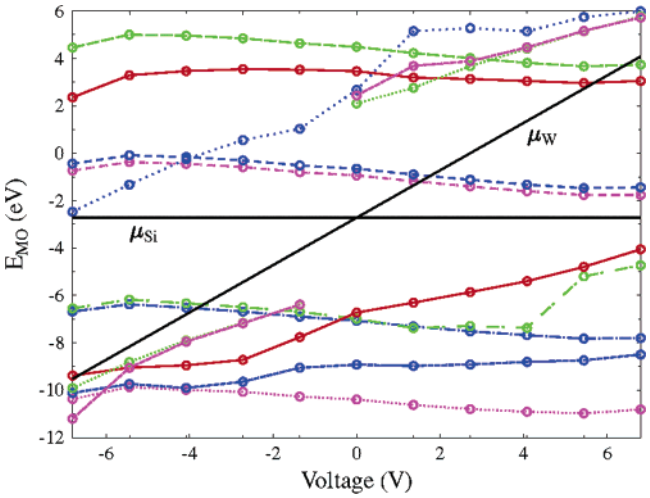

Figure 4. MO energies vs voltage drop.

the gap. As such, we expect to derive a qualitative description of the experimental images.

The current−voltage plot can be understood by considering the MO energy as a function of applied voltage, as shown in Figure 4. Current-carrying MOs are those that enter between the chemical potentials of the contacts (straight lines in the graph). Buildup of the current starts at the point where the MO crosses the chemical potential line (compare Figures 3 and 4). At negative bias voltages (where electrons flow from substrate to tip), the current mediating orbitals are the quasi-degenerate HOMO and HOMO−1 of the supermolecule, whereas at positive voltages (electrons flow from tip to substrate), the current-carrying orbitals are the quasi-degenerate LUMO and LUMO+1. However, essential current buildup begins when the HOMO−2 at negative voltage and LUMO+2 at positive voltage cross into the relevant energy regime (see explanation below).

Note that from the voltage-dependent behavior, it is easy to identify dominantly tip localized MOs as compared to those localized on the other side of the junction (molecule plus substrate) due to their characteristic voltage dependence. Note also that the MOs are voltage dependent. In particular, using Figure 4 as a guide and comparing probability densities at different voltages, the HOMO at zero volts becomes the HOMO−2 at $V \sim -6.5$ V (−0.25 au), the main current-carrying orbital at negative biases. The LUMO+2 at $V \sim +6.5$ V (+0.25 au), which dominates the current at positive bias, corresponds to the LUMO+5 at $V = 0$. The energy curves do not cross each other, and the avoided crossing regions are characterized

by mixed MOs. Indeed, the character of the orbitals can also change beyond the crossing regions.

To elucidate the nature of the MOs participating in the current transport, we compared the probability density distribution for the same molecule in the cases of open (NEGF-based) and closed (standard quantum chemical) calculations. We find strong similarity between the standard probability density of the closed system (square of the MO), calculated at $V = 0$, and the real part of the quasiprobability density calculated at a voltage drop of interest for the corresponding MO. The latter density is used to describe the probability density in the case of an open system (see discussion and examples below). This finding indicates the utility of the quasiprobability approach for describing the probability density of open quantum systems.

Similarity in the probability density distributions for the MOs of interest (HOMO−2 at $V \sim -6.5$ V and LUMO+2 at $V \sim +6.5$ V) computed for the closed and open systems indicates that the density obtained has a true "on-the-molecule" localization and does not arise as an artifact of the finite character of the sample. In the closed system, electron density cannot leave the structure (microcanonical ensemble), whereas the "openness" provides the possibility of partially adding or depleting electron density from the molecule so that it will be in equilibrium (or tend to be in equilibrium) with the external electron reservoirs. Only true on-the-molecule localization survives in the open case. Note also that to be able to judge the shape of the "electronic orbitals" relevant to STM experiments, it is essential to consider the "grand canonical ensemble" (open system) and to compute the probability density at the potential bias of interest. In general, the shapes of the MOs calculated for the same molecule when it is open, i.e., coupled to the contacts (with the Fermi energy in the middle of the HOMO−LUMO gap), as compared to the case when it is closed, are different. Differences might be important for molecules with high polarizability or small size (because of the enhanced propensity for these structures to "release" or "absorb" electronic charge).

To probe the effect of silicon cluster size, we analyzed the same molecule attached to a cluster of 36 silicon atoms. The probability density on the molecule remained unchanged for the MOs of interest (the current-carrying orbitals), suggesting that the cluster size used in the calculations is sufficient to reproduce the characteristics of the 1,3-cyclohexadiene mediated transport.

Figure 5 shows MO probability density for the HOMO−2 calculated at $V \sim -6.5$ V (HOMO at $V = 0$). This orbital is responsible for the current at negative voltage. It shows clear localization of the density probability on the carbon−carbon double bond. There is also localization on the 1 and 4 carbon atoms (the ones coupled to the Si surface) of the cyclohexadiene molecule. We identify this orbital of the supermolecule to be directly related to the π orbital of the carbon−carbon double bond. The reason for the identification is the proximity of the MO energies obtained in our NEGF calculation with the Gaussian MO at $V = 0$. In both cases, the MO is the HOMO, and the molecular orbital plot from the Gaussian calculation is shown in Figure 6. The two MOs higher in energy at $V \sim -6.5$ V (HOMO and HOMO−1) do not contribute to the current, due to the fact that those MOs are localized on the Si substrate (see Figure 7 for HOMO probability density at $V = -6.5$ V). We interpret these orbitals as indicators of the Si band edge, which would appear for a semi-infinite Si crystal. In this case, the electron has to tunnel through an effective barrier much wider than the one it would experience in the case of the MO

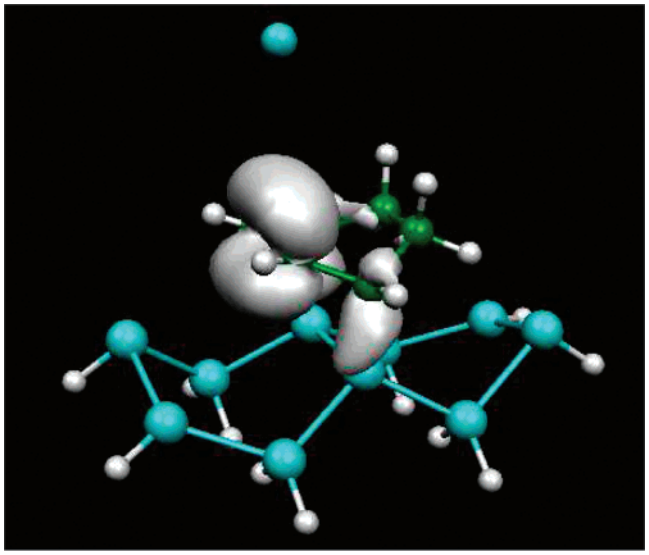

Figure 5. Probability density for the HOMO−2 calculated at $V \sim -6.5$ V (−0.25 au). This is the first main current-carrying orbital for negative voltage drops.

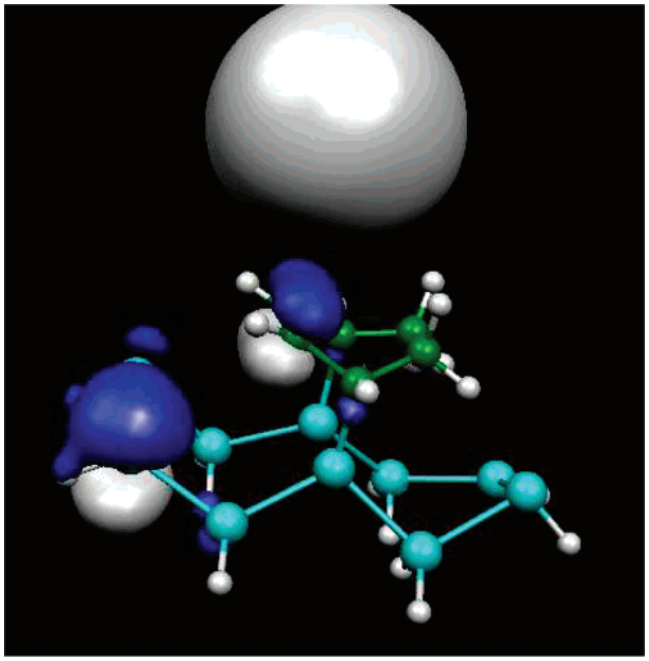

Figure 6. HOMO from Gaussian HF calculations, i.e., calculations at $V = 0$. This orbital corresponds to HOMO−2 at $V \sim -6.5$ V (−0.25 au).

presented in Figure 5. As a result, those two orbitals give almost no contribution to the current and are not visible in the experiment.

Figure 8 shows the MO probability density for the LUMO+2 calculated at $V \sim +6.5$ V (LUMO+5 at $V = 0$ V). This MO makes the main contribution to the current at positive voltage. Comparing its localization at the carbon−carbon double bond at $V \sim +6.5$ V with that of Gaussian based calculation for the LUMO+5 orbital at $V = 0$ V (see Figure 9), we conclude that this orbital contains the main contribution of the π^* carbon−carbon double bond. The situation with lower energy LUMO and LUMO+1 orbitals (both at zero voltage and $V \sim +6.5$ V), entering the relevant region at smaller positive voltages, is similar to that of the HOMO and HOMO−1 at negative voltages. Those are Si substrate localized orbitals of the Si crystal band edge, which do not participate strongly in the

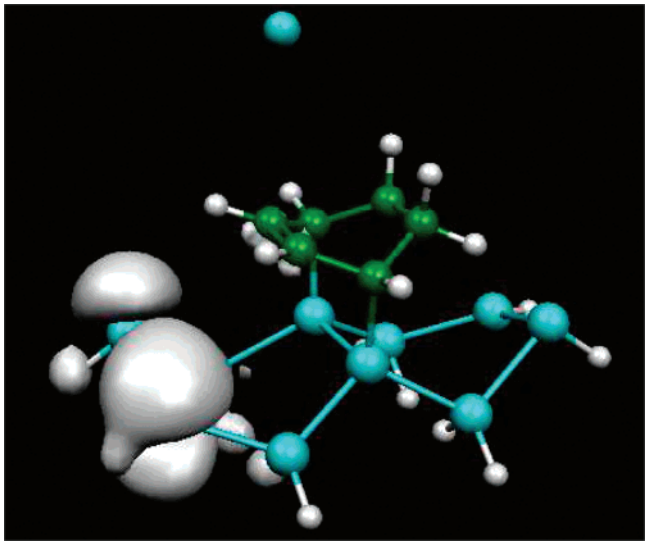

Figure 7. Probability density for the HOMO calculated at $V \sim -6.5$ V (-0.25 au). This orbital does not make essential contributions to the current because of its localization pattern.

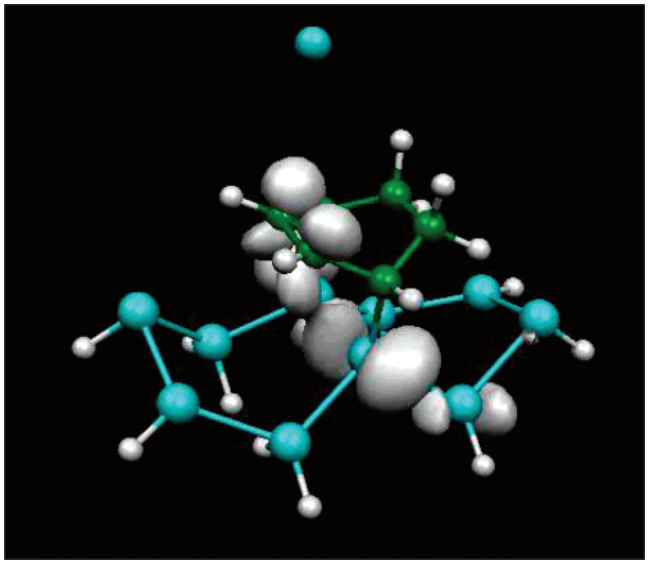

Figure 8. Probability density for the LUMO+2 calculated at $V \sim 6.5$ V ($+0.25$ au). This is the first main current-carrying orbital for positive voltage drop.

current due to the large effective energy barrier for electron tunneling.

Calculations at different bias voltages show robustness of the MO probability density shape in the range of voltages probed. However, the MO character may change with voltage. No significant changes in the MO shapes were found as the tip−molecule separation was varied. We calculated the MO density with the tip directly over the carbon−carbon double bond with the tip in van der Waals contact (~3 Å) and 4 Å from the molecular plane. Calculations were also performed on the molecule and silicon substrate with no tip. In all cases, the character of the relevant MOs appeared to be essentially unchanged (tip-localized orbitals were absent in the latter calculations), although at 3 Å separation significant delocalization of the probability density occurred between the tip and the supermolecule. The latter observation suggests that bringing the tip too close to the surface will blur the STM image.

Consider tip−molecule interactions modeled by tunneling through an effective barrier. The wider the barrier, the more focused the electron flow will be, because the transmission

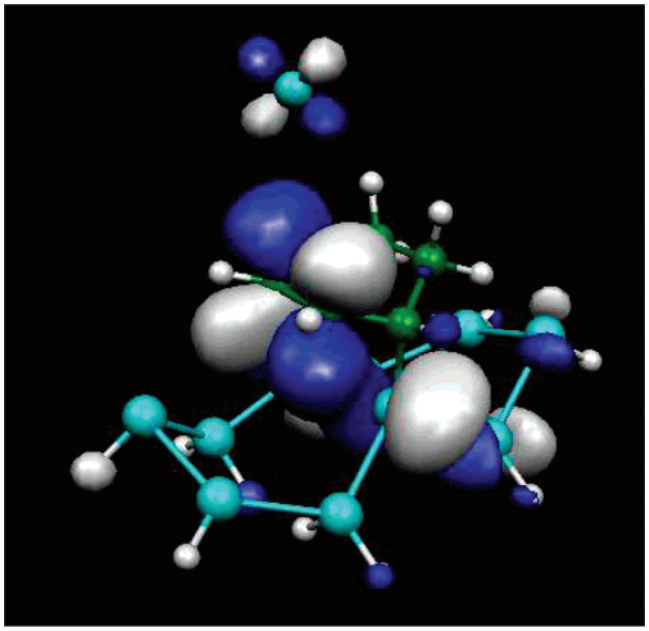

Figure 9. LUMO+5 from HF Gaussian calculations, i.e., calculations at $V = 0$. This orbital corresponds to LUMO+2 at $V \sim 6.5$ V ($+0.25$ au).

probability decreases exponentially with the barrier width; i.e., only "straight paths" survive. At the same time, the current drops with increasing tip−molecule distance. The sharpest image, therefore, is expected to appear at intermediate tip distances: not so close that electron flux is "unfocused", and not so far that the current is too weak to measure. Note that large tip−molecule separations refer to distances comparable to the dimensions of the molecule parallel to the surface. For extremely large distances (distances much greater than the molecular size), the electron path to any part of the molecule is essentially the same, making them indistinguishable. We expect the STM images for the case at hand to be determined by the orbital structure of the molecule−silicon substrate with the tip (position and distance) playing a minor role in the image shape, but an essential role in "focusing" the image.

The first current carrying orbital at negative voltage (HOMO−2 at $V \sim -6.5$ V) could be a candidate for obtaining the double bond image in the STM experiment for the geometry studied. However, the image sharpness could be degraded due to additional localization on the 1 and 4 carbon atoms (see Figure 5), which can lead to additional bright spots in the image. Similarly, the first current carrying orbital at positive voltage (LUMO+2 at $V = +6.5$ V) is a candidate for observing the double bond at positive voltage drop. Note that the image in this case is expected to be sharper due to the absence of additional localization on the cyclohexadiene molecule (see Figure 8). Importantly, the current at positive voltages is much larger than at negative voltages for the same absolute value of the voltage drop (see Figure 3), thus leading to a larger signal at positive voltages. We attribute this behavior partly to mixing of the corresponding MOs with the Si surface orbitals. In the case of the current-carrying MOs at positive voltage, this mixing is clearly seen in Figures 8 and 9. It is absent for the MO relevant for current flow in the case of negative voltage (see Figures 5 and 6). As a result, electrons at positive voltages have to tunnel only through the barrier between the tip and the carbon−carbon double bond localization, whereas at negative voltages the electrons encounter two barriers that diminish the current. This argument is supported by considering the imaginary part of the quasiprobability density for the two orbitals. Negative

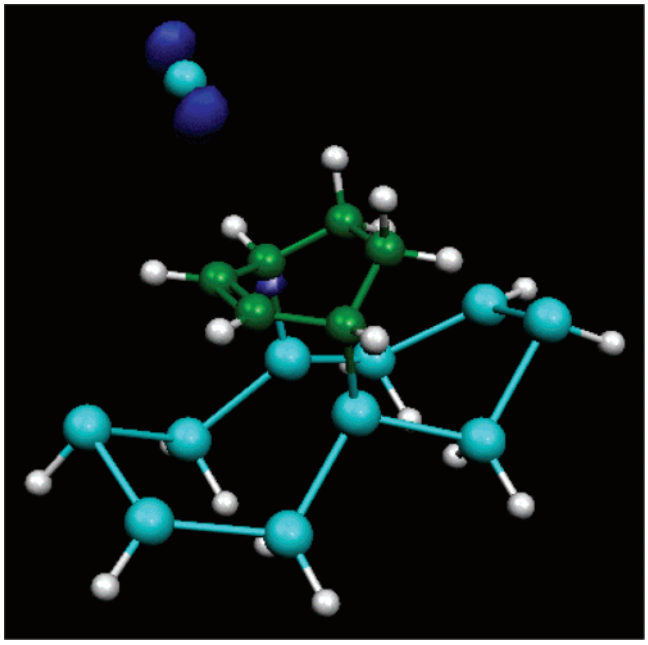

Figure 10. Imaginary part of the quasiprobability density for HOMO−2 calculated at $V \sim -6.5$ V (−0.25 au). This is the first main current-carrying orbital for negative voltage drops.

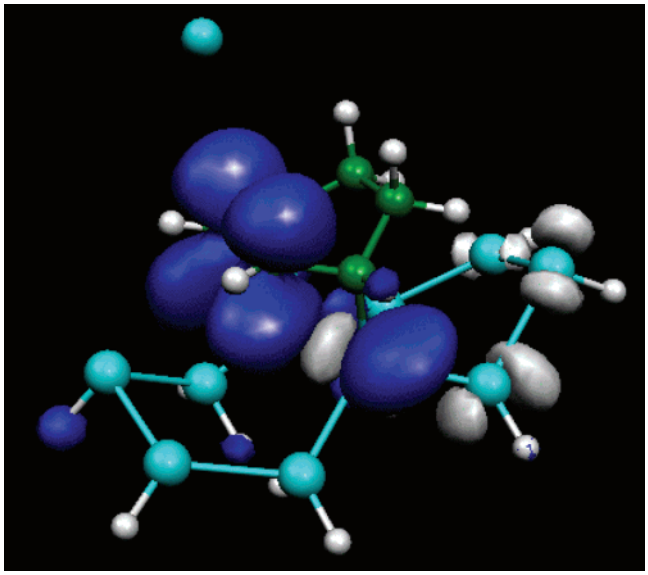

Figure 11. Imaginary part of quasiprobability density for the LUMO+2 calculated at $V \sim 6.5$ V (+0.25 au). This is the first main current-carrying orbital for positive voltage drops.

voltage current-carrying orbital shows almost zero imaginary part (see Figure 10), indicating strong localization of the MO on the molecule. Yet, the positive voltage current-carrying orbital has much weaker localization on the molecule (see Figure 11), indicating strong mixing with the Si cluster orbitals.

The physical reason for current−voltage asymmetry observed experimentally, and obtained in our calculations as stronger or weaker localization of the orbital on the molecule, may be due to molecular charging. Figure 12 shows the difference between the Mulliken charge on the molecular (C_8H_6) part of the supermolecule and the Si cluster ($Si_{10}H_{12}$) vs applied voltage. At zero bias the molecule acquires ~1.7*e* upon adsorption. The charging effect upon adsorption was predicted earlier and is due to high charge flexibility of dangling bonds.[51] For example, in experiments of C_{60} adsorbed on the Si surface, charge transfer (from the substrate to the molecule) of ~1 electron per dangling

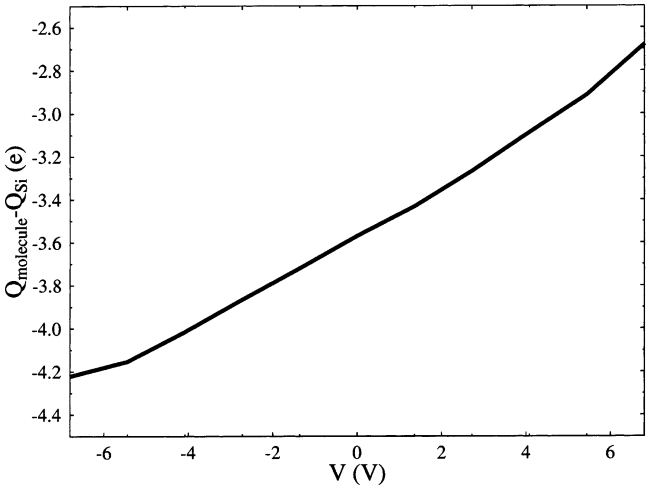

Figure 12. Difference between the Mulliken charge on molecule (C_8H_6) part of the supermolecule and the Si cluster ($Si_{10}H_{12}$).

bond interacting with the molecule was observed,[52] whereas ab initio study indicated partially ionic character of the Si−C bond.[53] This complies with our current observation. For negatively biased junctions, the molecule develops a strong negative charge relative to the Si crystal. Thus, a dipole is induced on the crystal surface, creating a depletion region and obstructing electron flow from the substrate to the molecule. Charging is much weaker for positive voltage biases, and because no dipole of opposite sign is developed, the surface dipole does not play an important role in this case. Similar effects of current rectification for clusters attached at Si surfaces were reported in ref 54.

In summary, two factors, the "purity" of the carbon−carbon double bond localization and the Si surface dipole (creating one more barrier to tunnel through) makes the double bond observation more favorable for positive (π^* mediated tunneling) rather than negative (π mediated tunneling) voltages.

5. Conclusion

STM experiments on 1,3-cyclohexadiene bonded to silicon (100) 2×1 were analyzed using a NEGF-HF approach. We described the molecular origin of the STM images and their bias dependence qualitatively. It is essential to perform calculations for the open quantum system at the desired voltages to explore the relevant (current-carrying) MOs and to take into account charging effects.

The tip position over the molecule does not play a substantial role in determining the MO shapes. Smearing out of the STM images is expected to arise for close tip distances due to strong tip-molecule mixing. In contrast, large tip−molecule distances are anticipated to lead to sharper 'focus' but smaller currents for distances of the order of the molecular size. For larger distances the image will be blurred. The overall resolution of the STM image will be determined by a tradeoff among these intrinsic effects.

The shape of the probability density for the current-carrying MOs controls the observed STM image. Thus, the observed STM images are approximated by a superposition of the images arising from the relevant MOs. LUMO+2 (at $V \sim +6.5$ V) responsible for observing the carbon−carbon double bond at positive voltages has π^* character. We stress that it is the ability of the π^* to mix with the Si surface (its "delocalized" character) that makes current flow through it more effective than through its π counterpart at opposite voltages. Physically, this effect arises from the dipole induced in the Si crystal surface by the

molecular attachment. The form of the MO localization on the cyclohexadiene molecule and current−voltage asymmetry due to the molecule-induced surface dipole leads to the observation of the carbon−carbon double bond in the STM experiments for positive but not negative bias voltages.

There are two new points in our consideration as compared to previous publications.[23,24] This work is a first example of application of complex quasiprobability in molecular junction properties calculation. As such, it is a step forward, because conventional molecular orbitals are not appropriate tools to deal with open quantum systems out of equilibrium. Second, rectification described in the current study has a completely different origin as compared to that described in ref 23. Though there the cause for signal rectification was localization of the HOMO on different sides of a break junction, here we have a surface dipole as a main source of asymmetry in STM images under opposite voltages.

Although we expect the effects described here to be robust, one could perform the self-energy analysis described in ref 48 to probe the impact of introducing a more realistic description for the silicon band structure. Calculations along these lines may lead to negative differential resistance effects as well.[48]

Acknowledgment. We thank the Keck Foundation for support of this project through the Center for Nanoscale Molecular Electronics at Duke and Pittsburgh. Additional support from the NEDO Foundation (Japan) is gratefully acknowledged. We thank Prof. John Boland and Dr. Lucile Teague for stimulating discussions of their experiments. M.G. thanks Prof. Abraham Nitzan for helpful discussion.

References and Notes

(1) Kagan, C. R.; Ratner, M. A. *MRS Bull.* **2004**, *29*, 376−384.
(2) Seideman, T.; Guo, H. *J. Theor. Comput. Chem.* **2003**, *2*, 439−458.
(3) Hush, N. S. *Ann. N. Y. Acad. Sci.* **2003**, *1006*, 1−20.
(4) Avouris, P. *Acc. Chem. Res.* **2002**, *35*, 1026−1034.
(5) *Molecular Electronics: A 'Chemistry of the 21st Century' Monograph*; Jortner, J., Ratner, M. A., Eds.; Blackwell Science: Oxford, U.K., 1997.
(6) *Molecular Electronics: Science and Technology*; Aviram, A., Ratner, M. A., Eds.; New York Academy of Sciences: New York, 1998.
(7) *Molecular Electronics II*; Aviram, A., Ratner, M. A., Mujica, V., Eds.; New York Academy of Sciences: New York, 2002.
(8) Lee, H. J.; Ho, W. *Science* **1999**, *286*, 1719−1722.
(9) Agrait, N.; Untiedt, C.; Rubio-Bollinger, G.; Vieira, S. *Phys. Rev. Lett.* **2002**, *88*, 216803.
(10) Schwab, K.; Henriksen, E. A.; Worlock, J. M.; Roukes, M. L. *Nature* **2000**, *404*, 974−977.
(11) Ranganathan, S.; Steidel, I.; Anariba, F.; McCreery, R. L. *Nano Lett.* **2001**, *1*, 491−494.
(12) Gaudioso, J.; Lauhon, L. J.; Ho, W. *Phys. Rev. Lett.* **2000**, *85*, 1918−1921.
(13) Caroli, C.; Comberscot, R.; Nozieres, P.; Saint-James, D. *J. Phys. C: Solid State Phys.* **1971**, *4*, 916−929.
(14) Caroli, C.; Comberscot, R.; Lederer, D.; Nozieres, P.; Saint-James, D. *J. Phys. C: Solid State Phys.* **1971**, *4*, 2598−2610.
(15) Caroli, C.; Comberscot, R.; Nozieres, P.; Saint-James, D. *J. Phys. C: Solid State Phys.* **1972**, *5*, 21−42.
(16) Kadanoff, L. P.; Baym, G. *Quantum Statistical Mechanics*; W. A. Benjamin, Inc.: New York, 1962.
(17) Keldysh, L. V. *Sov. Phys. JETP* **1965**, *20*, 1018−1026.
(18) Xue, Y.; Datta, S.; Ratner, M. A. *J. Chem. Phys.* **2001**, *115*, 4292−4299.
(19) Damle, P. S.; Ghosh, A. W.; Datta, S. *Phys. Rev. B* **2001**, *64*, 201403.
(20) Taylor, J.; Gui, H.; Wang, J. *Phys. Rev. B* **2001**, *63*, 121104(R).
(21) Taylor, J.; Gui, H.; Wang, J. *Phys. Rev. B* **2001**, *63*, 245407.
(22) Larade, B.; Taylor, J.; Mehrez, H.; Guo, H. *Phys. Rev. B* **2001**, *64*, 075420.
(23) Galperin, M.; Nitzan, A.; Sek, S.; Majda, M. *J. Electroanal. Chem.* **2003**, *550*−*551*, 337−350.
(24) Galperin, M.; Nitzan, A. *Ann. N. Y. Acad. Sci.* **2003**, *1006*, 48−67.
(25) Teague, L. C.; Boland, J. J. *J. Phys. Chem. B* **2003**, *107*, 3820−3823.
(26) Teague, L. C.; Chen, D.; Boland, J. J. *J. Phys. Chem. B* **2004**, *108*, 7827−7830.
(27) Teague, L. C.; Boland, J. J. Private communication.
(28) Hirose, K.; Tsukada, M. *Phys. Rev. B* **1995**, *51*, 5278−5290.
(29) Kobayashi, N.; Hirose, K.; Tsukada, M. *Jpn. J. Appl. Phys.* **1997**, *36*, Part 1, 3791−3795.
(30) Löwdin, P.-O. *J. Chem. Phys.* **1950**, *18*, 365−375.
(31) Frisch, M. J.; Trucks, G. W.; Schlegel, H. B.; Scuseria, G. E.; Robb, M. A.; Cheeseman, J. R.; Zakrzewski, V. G.; Montgomery, J. A., Jr.; Stratmann, R. E.; Burant, J. C.; Dapprich, S.; Millam, J. M.; Daniels, A. D.; Kudin, K. N.; Strain, M. C.; Farkas, O.; Tomasi, J.; Barone, V.; Cossi, M.; Cammi, R.; Mennucci, B.; Pomelli, C.; Adamo, C.; Clifford, S.; Ochterski, J.; Petersson, G. A.; Ayala, P. Y.; Cui, Q.; Morokuma, K.; Malick, D. K.; Rabuck, A. D.; Raghavachari, K.; Foresman, J. B.; Cioslowski, J.; Ortiz, J. V.; Baboul, A. G.; Stefanov, B. B.; Liu, G.; Liashenko, A.; Piskorz, P.; Komaromi, I.; Gomperts, R.; Martin, R. L.; Fox, D. J.; Keith, T.; Al-Laham, M. A.; Peng, C. Y.; Nanayakkara, A.; Gonzalez, C.; Challacombe, M.; P. M. W. Gill, P. M. W.; Johnson, B. G.; Chen, W.; Wong, M. W.; Andres, J. L.; Head-Gordon, M.; Replogle, E. S.; Pople, J. A. *Gaussian 98*, revision A.4; Gaussian, Inc.: Pittsburgh, PA, 1998.
(32) Saunders, V. R. *Molecular Integrals for Gaussian Type Functions*; In *Methods in Computational Molecular Physics*; Diercksen, G. H. F.; Wilson, S., Eds.; D. Reidel Publishing Company, 1983; NATO ASI Series, Vol. 113.
(33) Haug, H.; Jauho, A.-P. *Quantum Kinetics in Transport and Optics of Semiconductors*; Springer: Berlin, 1996.
(34) Datta, S. *Electronic Transport in Mesoscopic Systems*; Cambridge University Press: Cambridge, 1995.
(35) Nitzan, A. *Annu. Rev. Phys. Chem.* **2001**, *52*, 681−750.
(36) Meir, Y.; Wingreen, N. S. *Phys. Rev. Lett.* **1992**, *68*, 2512−2516.
(37) Galperin, M.; Nitzan, A.; Benjamin, I. *J. Phys. Chem. A* **2002**, *106*, 10790−10796.
(38) Landau, L. D.; Lifshitz, E. M. *Quantum Mechanics. Non-Relativistic Theory*; Pergamon Press: Oxford, U.K., 1965.
(39) Engdahl, E.; Maniv, T.; Moiseyev, N. *J. Chem. Phys.* **1988**, *88*, 5864−5870.
(40) Wolkow, R. A.; Lopinski, G. P.; Moffatt, D. J. *Surf. Sci.* **1998**, *416*, L1107−1113.
(41) No capping on the Si surface corresponds to the clean surface obtained in the experiment.[25,26] Note, however, that test Gaussian calculations done for the closed system did not reveal much difference for the capped vs uncapped Si surface structures.
(42) Tian, W.; Datta, S.; Hong, S.; Reifenberger, R.; Henderson, J. I.; Kubiak, C. P. *J. Chem. Phys.* **1998**, *109*, 2874−2882.
(43) Tersoff, J.; Hamann, D. R. *Phys. Rev. Lett.* **1983**, *50*, 1998−2001.
(44) Tersoff, J.; Hamann, D. R. *Phys. Rev. B* **1985**, *31*, 805−813.
(45) Guinea, F.; Tejedor, C.; Flores, F.; Louis, E. *Phys. Rev. B* **1983**, *28*, 4397−4402.
(46) López-Sancho, M. P.; López-Sancho, L. M.; Rubio, J. *J. Phys. F: Metal Phys.* **1984**, *14*, 1205−1215.
(47) López-Sancho, M. P.; López-Sancho, L. M.; Rubio, J. *J. Phys. F: Metal Phys.* **1985**, *15*, 851−858.
(48) Rakshit, T.; Liang, G. C.; Ghosh, A. W.; Datta, S. *arXiv: cond-mat* **2003**, 0305695.
(49) Wang, F.; Sorescu, D. C.; Jordan, K. D. *J. Phys. Chem. B* **2002**, *106*, 1316−1321.
(50) Yaliraki, S. N.; Roitberg, A. E.; Gonzalez, C.; Mujica, V.; Ratner, M. A. *J. Chem. Phys.* **1999**, *111*, 6997−7002.
(51) Lu, X.; Xu, X.; Wang, N.; Zhang, Q.; Lin, M. C. *Chem. Phys. Lett.* **2002**, *355*, 365−370.
(52) Suto, S.; Sakamoto, K.; Wakita, T.; Hu, Ch.-W.; Kasuya, A. *Phys. Rev. B* **1997**, *56*, 7439−7445.
(53) Masenelli, B.; Tournus, F.; Mélinon, P.; Pérez, A.; Blaze, X. *J. Chem. Phys.* **2002**, *117* 10627−10634.
(54) Bolotov, L.; Uchida, N.; Kanayama, T. *J. Phys.: Condens. Matter* **2003**, *15*, S3065−S3081.